Control Architecture for a Switched Doubly Fed Machine Propulsion Drive

Arijit Banerjee, *Student Member, IEEE*, Michael S. Tomovich, *Student Member, IEEE*, Steven B. Leeb, *Fellow, IEEE*, and James L. Kirtley, Jr., *Life Fellow, IEEE*

***Abstract*—Doubly fed machines (DFMs) are well known for limited-speed-range applications such as in wind power generation due to their reduced requirement in power electronic rating. Switched DFM drives offer the same benefit on power electronic requirement but operate on a wide speed range. This makes them attractive for wide-speed-range high-power applications, e.g., in ship propulsion. A unique controller is needed to fit the different demands of a switched DFM drive, specifically where both ac and dc supplies are available. This paper presents a control architecture for a switched DFM drive intended for propulsion application. The proposed architecture adapts to the on-the-fly changes in DFM configuration and seamlessly controls the speed/torque during these variations.**

***Index Terms*—Energy conversion, propulsion, reconfigurable architectures, rotating machine nonlinear analysis, rotating machine stability, stator flux estimation, torque control, variable-speed drives.**

NOMENCLATURE

ϵ	Rotor A-phase angle w.r.t stator A-phase axis (in radians).
$\overline{I}_s, \overline{I}_r$	Stator and rotor current space vectors (in amperes).
J, B	Total inertia (in kilogram square meter) and frictional coefficient (in newton meter second per radian).
T_1, T_2, T_3	Filter time constant (in seconds).
P	Number of poles.
R_s, R_r	Stator and rotor resistances (in ohms).
L_s, L_r, M	Stator, rotor, and mutual inductances (in henry).
Sw	Switching signal for ac–dc mode changeover.
τ, T_L	Electromagnetic and load torque (in newton meter).
$\overline{V}_{\rm ac}, \overline{V}_{\rm dc}$	AC and dc voltage space vectors (in volts).
$\overline{V}_s, \overline{V}_r$	Stator and rotor voltage space vectors (in volts).
ω, ω_e	Rotor speed (in mechanical radians per second and in electrical radians per second).
$\omega_s, \omega_{\rm ac}$	Stator flux frequency and ac supply frequency (in radians per second).
δ	Angle between the stator voltage and the stator flux vector.
$\overline{\psi}_s, \overline{\psi}_r$	Stator and rotor flux space vectors (in volt second).
Ψ_s, Δ	Steady-state stator flux magnitude and angle in ac mode.
$\psi_{s\alpha}, \psi_{s\beta}$	Stator flux components in $\alpha - \beta$ reference frame (in volt second).
ψ_s, θ_s	Stator flux magnitude $[\sqrt{(\psi_{s\alpha}^2 + \psi_{s\beta}^2)}]$ (in volt second) and angle $[\tan^{-1}(\psi_{s\beta}/\psi_{s\alpha})]$ w.r.t stator A-phase (in radians).
X_d, X_q	d- and q-axis components of any space vector $\overline{X}$.
$X_{\rm dc}, X_{\rm ac}$	Corresponding dc and ac mode values of variable X.
X^*	Reference value of variable X.

Manuscript received February 23, 2014; revised June 2, 2014; accepted July 8, 2014. Date of publication August 13, 2014; date of current version March 17, 2015. Paper 2014-IDC-0108.R1, presented at the 2013 IEEE Applied Power Electronics Conference and Exposition, Long Beach, CA, USA, March 17–21, and approved for publication in the IEEE TRANSACTIONS ON INDUSTRY APPLICATIONS by the Industrial Drives Committee of the IEEE Industry Applications Society. This work was supported in part by the Electric Ship Research and Development Consortium under The Office of Naval Research and in part by The Grainger Foundation and the MIT-SkTech SDP program.

The authors are with the Department of Electrical Engineering and Computer Science, Massachusetts Institute of Technology, Cambridge, MA 02139 USA (e-mail: arijit@mit.edu; tomovich@mit.edu; sbleeb@mit.edu; kirtley@mit.edu).

Color versions of one or more of the figures in this paper are available online at http://ieeexplore.ieee.org.

Digital Object Identifier 10.1109/TIA.2014.2347452

I. INTRODUCTION

CONVENTIONAL variable-speed drives typically operate from a dc bus, i.e., a converter controls and operates an electric machine by consuming and shaping power from a dc bus. When dc input power is naturally available, e.g., in an electrical vehicle where batteries or a fuel-cell may serve as a storage source, this approach can be attractive. For transportation systems with ac generation [1] and where ac power is desirable for other loads besides motive power (e.g., on a ship), providing a dc bus for a variable-speed drive can be an expensive proposition. This approach requires total conversion of the ship's generated power to dc and then reconstruction of variable ac waveforms using an inverter. A significant investment in power electronics is required, not only for the inverter bus also for the power-factor corrected rectifier likely needed to interface with the ac generator.

A doubly fed machine (DFM) offers a way to construct a variable-speed drive without processing every joule of shaft power from a dc bus [2]. The usage of power converters to handle only the slip power has led to the predominant usage of DFMs in reduced-speed-range applications such as in wind power generation [3] and in flywheel energy storage [4], [5]. For example, a typical wind generation DFM drive has one-third power electronics rating compared to the DFM power rating.

However, a wide operating speed range is required in a propulsion application including operation at zero speed. The advantage of the conventional DFM drive is lost because, in this case, the power electronic converter rating must be equal to that of the DFM. Other approaches like feeding the DFM

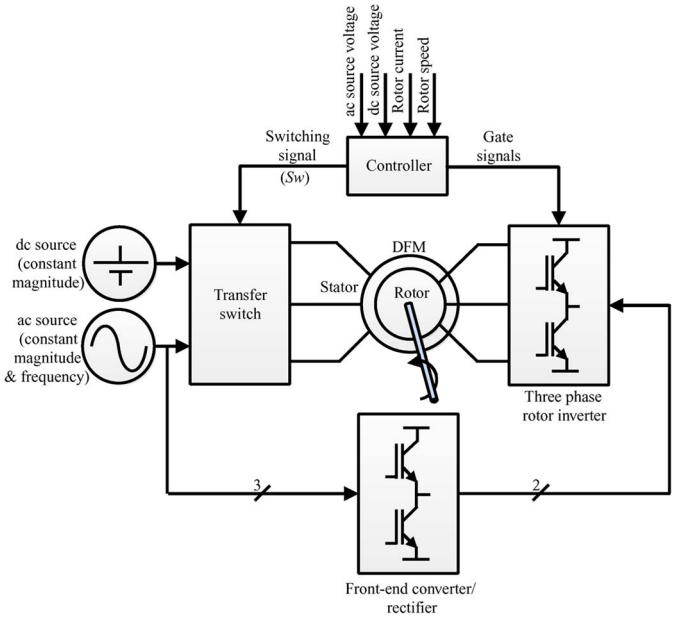

Fig. 1. Proposed configuration of a switched DFM drive.

with controlled double inverters on both windings increase the speed range with rated torque capability at all speeds [6], [7]. Although this has the advantage of having complete control on both the stator and the rotor excitation [7]–[11], the total power electronic converter rating matches with the rated mechanical shaft power.

Reconfiguring the DFM drive on-the-fly increases the operating speed range without sacrificing the advantage of reduced power electronics. This "switched DFM" class of drives essentially behaves as different conventional electrical machines based on the operating speed. One of the proposed approaches includes operation of the DFM as an induction machine at low speeds and as grid-connected doubly fed induction machine at high speeds [12], [13]. An alternative approach at lower speeds is to operate the DFM as a synchronous machine [14]. The proposed configuration is shown in Fig. 1. The drive has two sources (fixed frequency ac from the prime mover/generator and low voltage dc), either one of which can be connected to the stator through a transfer switch. The rotor is connected to a power electronic converter that can make variable frequency ac power. In dc or low-speed mode—in which the stator is connected to the dc supply—the DFM behaves like a separately excited synchronous machine. Stationary magnetic field in the stator reduces structural noise of the DFM, which is crucial in naval applications [15]. In ac or high-speed mode—in which the stator is connected to the ac supply—the machine behaves like a standard doubly fed induction machine, analogous to a windmill generator. The mode changeover is made depending on the operating rotor speed and designed transition speed.

The proposed switched DFM drive has significantly different challenges from a control perspective compared to a standard grid-connected doubly fed induction machine [16]–[21] or a wound rotor synchronous machine [22]. The rotor power electronic control has to adapt to the change in the machine configuration on-the-fly and should be able to control the individual modes (dc or ac) of the drive operation. Inappropriate mode transition can lead to undesirable speed/torque variation at the shaft [12]. This limitation has often led to the usage of the switched DFM drive in applications with two discrete operating regions instead of a standard high-power drive [13]. As the excitation in the stator undergoes a step change during mode changeover, the control scheme must ensure a stable and "bumpless" transition such that the coupled mechanical load and electrical sources are subjected to minimal disturbances. The proposed drive has to operate with a dc stator flux at low speed, which makes stator flux estimation challenging in the presence of measurement offset and drift. In addition, all of this must work in the context of a propulsion load that can experience sudden disturbances of load torque. This paper addresses these aforementioned challenges and proposes an architecture that can ensure a seamless control for the DFM drive at all operating modes including the instance of mode transition. In addition, the DFM can provide controllable power factor to an ac grid or ship microgrid which is also explored in this paper.

II. Operational Benefits of Switched DFM Drives

Neglecting leakages and winding resistances of the DFM, for a specific stator flux magnitude $\psi_{\rm sdc}$, the required rotor voltage is proportional to the *rotor speed* in dc mode and is given by

$$|v_r|_{\rm dc} = |\omega_e|\psi_{\rm sdc}. \tag{1}$$

In ac mode, the stator flux magnitude is set by the ac source voltage and frequency. Assuming the stator flux magnitude to be $\psi_{\rm sac}$, the required rotor voltage is proportional to the *rotor slip speed* and is given by

$$|v_r|_{\rm ac} = |\omega_{\rm ac} - \omega_e|\psi_{\rm sac}. \tag{2}$$

The stator flux magnitude in the dc mode is a design choice that is directly influenced by the required torque capability in low-speed operation. For ship propulsion, the load torque is proportional to the square of the operating speed. This implies that a lower torque capability at lower speed may be sufficient for the drive. In this case, the dc mode stator flux can be less than the ac mode stator flux. In other applications where a rated torque capability is required for the drive even at lower speeds, identical magnitudes of operating stator flux in dc as well as in ac mode are necessary.

Assuming equal stator flux magnitudes in both modes, (1) and (2) are normalized with respect to $\omega_{\rm ac}\psi_{\rm sac}$. The normalized required rotor voltage is plotted against the normalized rotor speed as shown in Fig. 2. A transition between the modes at 0.5 p.u. rotor speed will ensure that the maximum required rotor voltage is 0.5 p.u. while the drive operates in 0–1.5 p.u. speed range. Assuming the current rating of the rotor power electronics to be 1 p.u., the power sharing between the stator and rotor at different speeds is also plotted in Fig. 2. The rotor power electronics needs to control only 0.5 p.u. power, while the maximum mechanical power that is delivered at the shaft is 1.5 p.u. at maximum speed.

In a practical DFM, the dc source has to supply only the resistive losses in the stator. Therefore, the rating of the dc

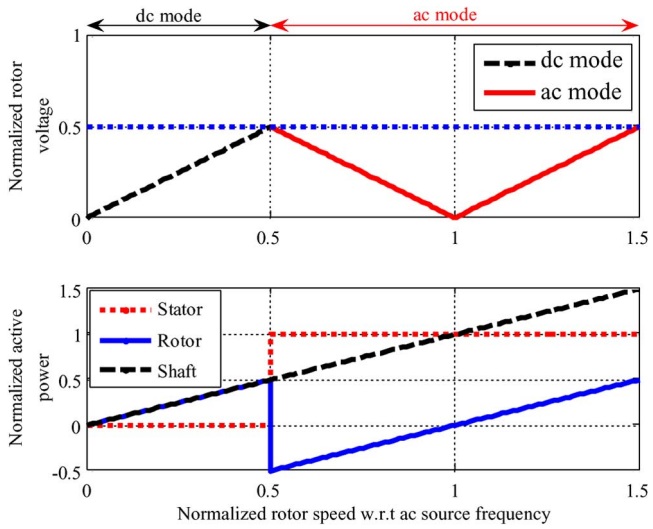

Fig. 2. Maximum power flow in the rotor is one-third of the maximum shaft power with 0–1.5 p.u. operating speed range for an ideal DFM.

source is a small fraction of the DFM power rating. The dc source is similar to an exciter in a synchronous generator. However, no control capability of the dc source is required in the proposed configuration, making it easy to construct from the ac source using a transformer-diode rectifier.

Apart from reducing the required rotor converter rating, the proposed drive also offers benefits on efficiency, output/EMI filter rating, and dc bus capacitor rating. DFM drives for wind turbines are known for better efficiencies of the power converter, as only one-third of the total power is processed by the converter compared to a full converter drive [23]. Similar benefits in efficiency are expected from the proposed switched DFM drive. Reduction of the required dc bus voltage to control the drive over the complete speed range directly translates into reduction of conduction and switching losses in the converter. In high-power applications, where available device rating limits the power handling capacity of the converter, the proposed drive architecture extends the capability limit of the drive without sacrificing the speed range [24].

III. Control Architecture for a Switched DFM

The proposed control architecture is based on the indirect field-oriented control. A doubly fed induction machine for wind application is traditionally controlled in the stator flux orientation [17] or the natural flux/grid flux orientation [18]. In a propulsion application, e.g., onboard a ship with a fixed voltage and frequency ac service, ignoring winding resistance, the stator flux will be fixed during ac mode by the ship ac service. The rotor inverter can be used to strictly control the shaft torque. Based on the remaining drive capability, the rotor inverter can also share the magnetizing current and control the stator power factor. In dc mode, the stator flux is set by both the stator and rotor magnetizing current. As the stator dc source is uncontrolled, the rotor inverter must ensure a desired stator flux level and then command the necessary torque. To control both modes seamlessly, it makes sense therefore to model the machine in a reference frame oriented to the stator flux.

A. DFM Model in Stator Flux Orientation

A DFM in the stator flux reference frame can be described using standard electrical machine equations [25]. The stator flux axis coincides with the d-axis, and the q-axis leads it by 90°. The electrical dynamics of the DFM are governed by

$$\frac{d}{dt}\psi_s = V_{sd} - R_s I_{sd} \tag{3}$$

$$\frac{d}{dt}\psi_{rd} = V_{rd} - R_r I_{rd} + (\omega_s - \omega_e)\psi_{rq} \tag{4}$$

$$\frac{d}{dt}\psi_{rq} = V_{rq} - R_r I_{rq} - (\omega_s - \omega_e)\psi_{rd} \tag{5}$$

$$\omega_s = \frac{d\theta_s}{dt} = \frac{V_{sq} - R_s I_{sq}}{\psi_s}. \tag{6}$$

The electromagnetic torque is governed by

$$\tau = -\frac{3}{2}\frac{P}{2}\frac{M}{L_s}\psi_s I_{rq}. \tag{7}$$

The flux linkage equations are

$$\psi_s = L_s I_{sd} + M I_{rd} \tag{8}$$

$$0 = L_s I_{sq} + M I_{rq} \tag{9}$$

$$\psi_{rd} = L_r I_{rd} + M I_{sd} \tag{10}$$

$$\psi_{rq} = L_r I_{rq} + M I_{sq}. \tag{11}$$

A simplified mechanical load equation is

$$J\frac{d\omega}{dt} + B\omega = \tau - T_L. \tag{12}$$

For a ship propulsion load, J will include the shaft, entrained water, and ship inertia.

B. Control Architecture Block Diagram

The control architecture for the proposed drive comprises two sections.

1) The stator flux magnitude ψ_s, stator flux angle θ_s (with respect to the stator A-phase axis), and stator flux frequency ω_s are estimated based on the measurement of the ac and dc source voltages, rotor current, and rotor mechanical speed, as shown in Fig. 3. The estimated stator flux angle is used to transform relevant variables to the stator flux reference frame. In steady state, the stator flux frequency is zero in dc mode and is equal to the ac source frequency in ac mode. However, at mode changeover, the stator flux frequency goes through a transient. Estimating the stator flux frequency enables smooth torque production under all operating conditions by providing appropriate feedforward terms for the rotor current controllers.
2) The commands to the rotor inverter and the stator source transition Sw are generated based on the estimated internal variables, terminal measurements, and reference set points, as shown in Fig. 4. Full mechanical control of the DFM is achieved from the rotor.

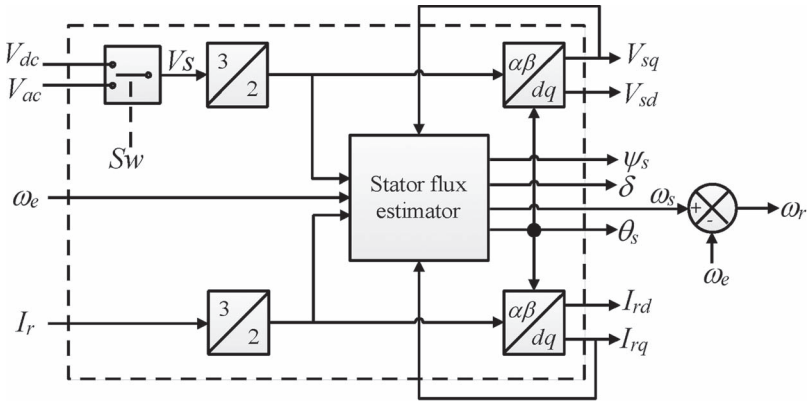

Fig. 3. Estimation of machine internal variables based on terminal measurements required for the proposed control architecture.

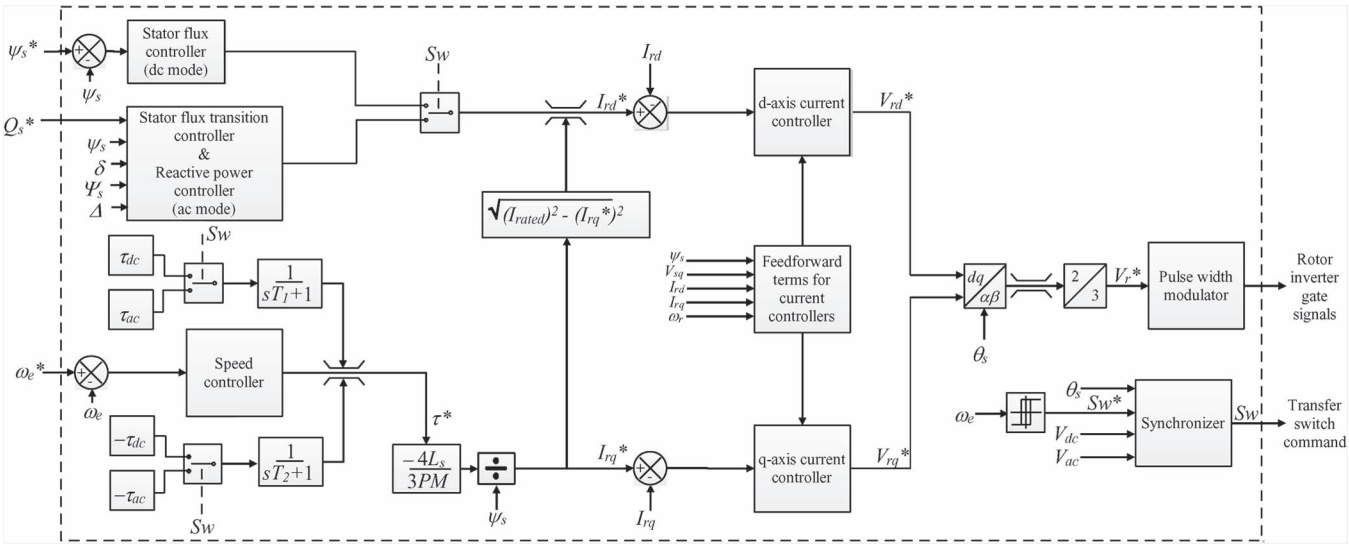

Fig. 4. Control architecture of the proposed DFM drive using the estimated machine internal variables and terminal measurements to command the rotor inverter and the stator transfer switch based on the reference set point.

The rotor q-axis current reference is generated depending on the desired torque. Based on the required drive torque–speed characteristic, the drive may be designed to have different torque capability in low- and high-speed regions. This results in different saturation limits at the output of the speed controller $\tau_{\rm dc}$ or $\tau_{\rm ac}$ based on the operating mode as shown in Fig. 4. The torque limits are transitioned with a low-pass filter of appropriate cutoff frequency during mode transition. This avoids a step change in the demanded q-axis current when the drive is operating at its peak torque capability while undergoing a mode transition. For example, in a drive designed with lower torque capability in dc mode compared to ac mode, the time-constant T_1, relevant during acceleration, is chosen to be equal to or slower than the DFM stator time constant. This allows the stator flux to settle to a steady value in ac mode before a higher torque is demanded. However, the time-constant T_2, relevant during braking, is chosen to be significantly faster than the DFM stator time constant.

The rotor d-axis current I_{rd} performs different functions during the two modes. In dc mode, I_{rd} is used to maintain the stator flux magnitude. In ac mode, I_{rd} is used to control the stator reactive power within the ratings of the rotor power electronic converter. Thus, based on the operating mode, I_{rd}^* is generated from either the stator reactive power controller or the stator flux controller. The rotor d-axis current limit is based on the commanded rotor q-axis current such that the DFM/rotor power electronic converter current rating $I_{\rm rated}$ is not exceeded during any of the operating modes as shown in Fig. 4.

The stator flux vector is stationary in dc mode and rotates at the ac source frequency in ac mode relative to the stator reference frame. The stator flux magnitude may also differ in the two modes based on the drive design. At the instant of mode transition, the stator flux undergoes transients which directly impacts the shaft torque and the power transients seen by the ac source. Two degrees of freedom can be utilized to ensure that the stator flux is minimally perturbed. The first degree of freedom is the switching instant at which the stator connection of the DFM is changed between the dc and ac sources. This is appropriately chosen by the synchronizer, shown in Fig. 4, which commands binary signal Sw to the transfer switch. Based on the relative magnitude of the designed transition speed and the actual mechanical speed of the rotor, a transition command Sw^* is generated. Sw^* is fed to the synchronizer

along with the estimated stator flux angle and the measured ac and dc source voltages that compute Sw.

The remaining degree of freedom to suppress the stator flux oscillation during the mode transition is by actively commanding the d-axis rotor current. This is achieved by appropriate design of the stator flux controller (effective in dc mode) and the stator flux transition controller (effective in ac mode).

C. Stator Flux Estimator

The most important aspect of stator-flux-oriented control is the estimation of stator flux magnitude and angle under all operating conditions. In a DFM, the stator flux is generally estimated either through a voltage model based on the differential equations or a current model based on the flux linkage equations [26]. Alternatively, the stator flux can be estimated from the stator voltage vector by assuming that it lags the voltage by 90° [17]. As the proposed drive configuration undergoes voltage and flux transients, this assumption need not be always true. The voltage model incorporates integrators in the stationary reference frame $\alpha\beta$ given by

$$\psi_{s\alpha} = \int (V_{s\alpha} - R_s I_{s\alpha})dt$$

$$\psi_{s\beta} = \int (V_{s\beta} - R_s I_{s\beta})dt. \tag{13}$$

In ac mode, the integrators can be approximated with low-pass filters in practical implementations [25], avoiding problems with measurement offset and drift in the integral computations [26]. The cutoff frequency of these low-pass filters must be well below the signal frequency. However, this approximation of the integral with a low-pass filter remains impractical in dc mode, where the signal frequency is zero.

The estimation problem in both modes can be greatly simplified by computing the stator flux with a hybrid estimator that uses flux linkage equations (a current model) augmented with the voltage model (13). Using stator flux equation (current model) in (13) to replace the stator current yields

$$\overline{V}_s = \frac{R_s}{L_s}(\overline{\psi_s} - M\overline{I_r}e^{j\varepsilon}) + \frac{d}{dt}\overline{\psi_s}. \tag{14}$$

The rotor current in the stationary reference frame is given by

$$I_{r\alpha} + jI_{r\beta} = \overline{I_r}e^{j\varepsilon}. \tag{15}$$

Using (15) in (14) and rearranging real and imaginary parts give

$$\frac{d}{dt}\psi_{s\alpha} + \frac{R_s}{L_s}\psi_{s\alpha} = V_{s\alpha} + \frac{R_s M}{L_s}I_{r\alpha}$$

$$\frac{d}{dt}\psi_{s\beta} + \frac{R_s}{L_s}\psi_{s\beta} = V_{s\beta} + \frac{R_s M}{L_s}I_{r\beta}. \tag{16}$$

These expressions for the components of stator flux are governed by first-order differential equations that correspond to "low-pass" transfer functions relating the "input" voltages and currents to the "output" fluxes. This flux estimator is attractive, as its low-pass quality can minimize the effect of voltage and current measurement noise.

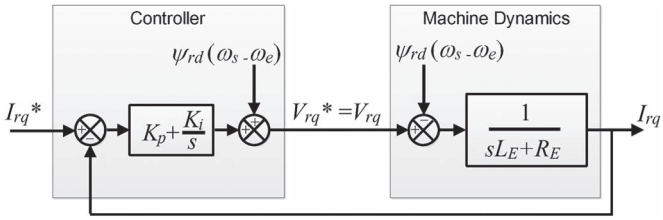

Fig. 5. Block diagram for the design of q-axis current controller: K_p and K_i are chosen based on the first-order plant model.

By avoiding the direct use of stator current in the flux estimator, a mechanism for potentially detecting parameter variations as the machine operates is preserved. Based on the estimated stator flux and the measured rotor currents, the stator currents can be estimated using (8) and (9). A direct measurement of the stator currents can potentially be compared against the estimated values to verify the stator flux estimation. Disagreement between the measured and estimated stator currents can be used to trigger the need for *in situ* revision of the machine parameters.

Apart from the stator flux magnitude and angle, other necessary estimated variables for proper control of the proposed drive include the stator flux frequency and the angle δ, defined as the angle between the stator flux vector and the stator voltage vector. While δ can be easily calculated based on the estimated stator flux angle and the measured stator voltage, the stator flux frequency can be estimated from the transformed stator voltage, rotor current, and DFM parameters using (6) and (9).

D. Design of the Rotor Current and Speed Controller

Both dc and ac modes require a feedback loop to control the speed and the d- and q-axis rotor currents. The q-axis current controller can be designed using (9) and (11) to find ψ_{rq} in terms of I_{rq}, thereby substituting the result in (5). The equation governing the q-axis rotor current dynamics is

$$V_{rq} = \underbrace{R_r}_{R_E} I_{rq} + \underbrace{\left(L_r - \frac{M^2}{L_s}\right)}_{L_E}\frac{d}{dt}I_{rq} + (\omega_s - \omega_e)\psi_{rd}. \tag{17}$$

The drive V_{rq} is provided by the rotor inverter. The desired V_{rq}^* is computed as the output of a proportional-integral (PI) compensator added to a speed voltage term that cancels the cross-coupling effect of ψ_{rd} in (17). ψ_{rd} is indirectly estimated using (8) and (10) as

$$\psi_{rd} = \left(L_r - \frac{M^2}{L_s}\right)I_{rd} + \frac{M}{L_s}\psi_s. \tag{18}$$

The overall q-axis current controller along with the involved machine dynamics based on (17) is shown in Fig. 5. Proportional and integral gains (K_p and K_i) of the controller are chosen to ensure loop stability, desired transient response, and acceptable steady-state error.

The design of the d-axis current controller is similar. Equations (18) and (3) are used in (4), which is translated to

measured or estimated variables using (8)–(11) to obtain

$$V_{rd} = \left(R_r + \frac{R_s M^2}{L_s^2}\right) I_{rd} + \left(L_r - \frac{M^2}{L_s}\right) \frac{d}{dt} I_{rd} + \underbrace{\frac{M}{L_s} V_{sd} - \frac{R_s M}{L_s^2} \psi_s - (\omega_s - \omega_e) \left(L_r - \frac{M^2}{L_s}\right) I_{rq}}_{\text{Equivalent Voltage Terms}}. \quad (19)$$

This equation is used to design a d-axis current controller with a PI compensator. The equivalent inductance and resistance of the machine dynamics L_E and R_E are appropriately changed in Fig. 5 using (19) to design K_p and K_i for the PI compensator. The "equivalent voltage" terms are added to the PI compensator output.

Finally, the shaft speed control is designed using (12) and by noting that the electromagnetic torque is related to the q-axis rotor current through (7). The bandwidth of the speed controller is chosen such that it is much slower than the q-axis current controller bandwidth. This is a design choice that will determine the final performance of the propulsion drive. A PI compensator stabilizes the speed loop in the experiments presented in this paper.

E. Design of the Stator Flux Controller in DC Mode

In dc mode, the stator flux magnitude for the DFM needs to be completely controlled through the rotor since the dc voltage source connected to the stator is uncontrolled. Using (8) in (3)

$$I_{rd} = \frac{L_s}{M R_s} \frac{d}{dt} \psi_s + \frac{1}{M} \psi_s - \underbrace{\frac{L_s}{M R_s} V_{sd}}_{\text{Voltage term}}. \quad (20)$$

A PI compensator responsive to the estimated flux error is used along with the voltage term to control the d-axis rotor current and, therefore, the stator flux magnitude. The previously discussed rotor d-axis current compensator is a minor loop within the stator flux controller, as shown in Fig. 4. Therefore, the bandwidth of the flux controller is chosen such that it is significantly lower than the d-axis current controller.

F. Design of the Reactive Power Controller in AC Mode

In ac mode, the stator flux magnitude is predominantly set by the ac source voltage and frequency. Assuming a negligible stator resistance in (3) and (6)

$$\psi_s = \frac{V_{sq} - R_s I_{sq}}{\omega_s} \approx \frac{V_{sq}}{\omega_s} \approx \frac{V_{\text{ac}}}{\omega_{\text{ac}}}. \quad (21)$$

The d-axis rotor current in this mode is commanded to control the flow of stator reactive power to and from the ac mains as in a standard wind turbine application [19]. Any desired stator reactive power, within the machine and inverter limits, can be provided according to

$$Q_s = \frac{3}{2}(V_{sq} I_{sd} - V_{sd} I_{sq}). \quad (22)$$

Substituting stator current components in terms of rotor currents using (8) and (9) in (22) and rearranging, the required rotor d-axis current necessary to command the steady-state reactive power flow on the stator can be computed as

$$I_{rd}^* = \left(\frac{1}{M} \psi_s + \frac{V_{sd}}{V_{sq}} I_{rq} - \frac{2}{3} \frac{L_s}{M V_{sq}} Q_s^*\right). \quad (23)$$

G. Design of the Stator Flux Transition Controller During DC to AC Mode Transition

During dc to ac mode transition, the stator flux moves from being controllable from the rotor to a state set by the ac supply. While the q-axis rotor current is completely devoted to torque/speed control of the DFM, only the d-axis rotor current is available to affect the magnitude and frequency of the stator flux during the transition.

Assuming a high current controller bandwidth, a simplified nonlinear plant model of the DFM during a dc to ac mode transition can be developed to design the stator flux transition controller. Rearranging (20),

$$\frac{d}{dt} \psi_s = -\frac{R_s}{L_s} \psi_s + V_{sd} + \frac{M R_s}{L_s} I_{rd}. \quad (24)$$

Replacing the q-axis rotor current in (6) using (7) yields

$$\omega_s = \frac{V_{sq}}{\psi_s} - \frac{1}{\psi_s^2} \frac{4 R_s}{3P} \tau. \quad (25)$$

After the stator connection is switched to the ac source, the angle between the stator flux vector and the stator voltage vector δ can be computed as

$$\frac{d\delta}{dt} = \omega_{\text{ac}} - \omega_s \quad (26)$$

and of course, the total stator voltage vector magnitude is equal to the resultant from the d-axis and q-axis components

$$V_{sd}^2 + V_{sq}^2 = \left|\overline{V_{\text{ac}}}\right|^2; V_{sq} = V_{\text{ac}} \sin\delta; V_{sd} = V_{\text{ac}} \cos\delta. \quad (27)$$

Using (24)–(27), the nonlinear DFM plant model can be described in state-space form as

$$\frac{d}{dt} \begin{bmatrix} \psi_s \\ \delta \end{bmatrix} = \begin{bmatrix} -\frac{R_s}{L_s} \psi_s + V_{\text{ac}} \cos\delta \\ \omega_{\text{ac}} - \frac{V_{\text{ac}} \sin\delta}{\psi_s} + \frac{1}{\psi_s^2} \frac{4 R_s}{3P} \tau \end{bmatrix} + \begin{bmatrix} \frac{M R_s}{L_s} \\ 0 \end{bmatrix} I_{rd}. \quad (28)$$

The model is equivalent to the well-known model [27] that has been used in grid-connected doubly fed induction generator stability studies, except that the q-axis current is replaced with the electromagnetic torque. Equating individual rows of (28) to zero results in the null-clines [28] for the plant in the state plane diagram as shown in Fig. 6. The intersection of the two null-clines determines the target steady-state operating point in ac mode of operation denoted by B in Fig. 6.

The dc mode stator flux magnitude and the instant of switching given by Sw determine the initial condition for the states in (28). For example, an operating dc mode stator flux level of 0.75 p.u. (normalized to the no-load ac mode stator flux) is considered. Switching from dc mode to ac mode at the instant when the incoming ac source voltage vector leads the

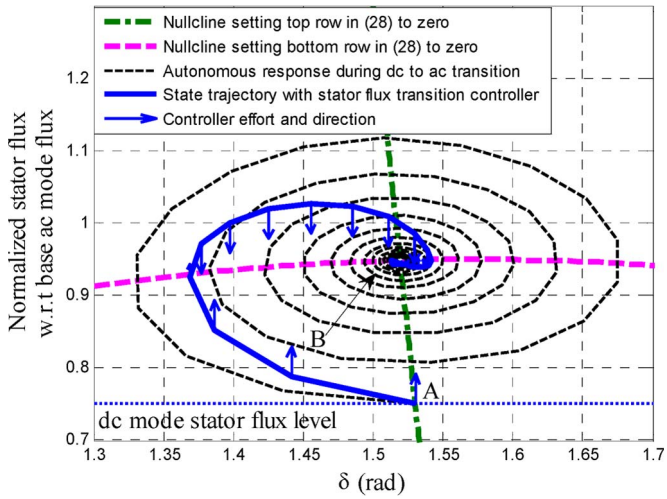

Fig. 6. State plane analysis: trajectory of stator flux magnitude and angle in the state plane during dc to ac mode transition. A corresponds to the initial state, while B is the target state for ac mode operation.

stator flux vector by 86° sets the initial state of the nonlinear plant described by (28) to be at A, as shown in Fig. 6. The autonomous response of the nonlinear plant during the dc to ac mode transition with the d-axis rotor current command set to zero and constant torque command forms a spiral in the state plane, suggesting a stable transition. However, there are two important observations. First, as the stator flux goes through the transition, the magnitude increases beyond the rated operating flux. If the stator flux that can be handled by the rotor inverter is higher than the designed value, the rotor power electronics will be voltage limited and will not be able to control the rotor current, resulting in undesirable torque and power disturbances. Second, there is sloshing of power back and forth between the stator and the ac power supply each time the stator flux goes above and below the steady-state flux level, respectively.

A stator flux transition controller is designed to affect the trajectory of the states of the simplified model during the mode transition and to damp the stator flux oscillations. This is a full-state feedback controller with estimated state variables setting the d-axis rotor current command. The nonlinear plant model, described by (28), is linearized across the ac steady-state operating point to design the controller gains. The linearized model obtained is

$$\frac{d}{dt}\begin{bmatrix}\tilde{\psi}_s\\ \tilde{\delta}\end{bmatrix}=\begin{bmatrix}-\frac{R_s}{L_s} & -V_{\rm ac}\sin\Delta\\ \frac{V_{\rm ac}\sin\Delta}{\Psi_s^2}-\frac{1}{\Psi_s^3}\frac{8R_s}{3P}\tau & -\frac{V_{\rm ac}\cos\Delta}{\Psi_s}\end{bmatrix}\begin{bmatrix}\tilde{\psi}_s\\ \tilde{\delta}\end{bmatrix}+\begin{bmatrix}\frac{MR_s}{L_s}\\ 0\end{bmatrix}\tilde{I}_{rd} \quad (29)$$

while the ac mode steady-state operating point is given by

$$\Psi_s\approx\frac{V_{\rm ac}}{2\omega_{\rm ac}}\left[1+\sqrt{1-\frac{4R_s\omega_{\rm ac}}{3PV_{\rm ac}^2}\tau}\right];\Delta=\cos^{-1}\left(\frac{R_s\Psi_s}{L_sV_{\rm ac}}\right). \quad (30)$$

Using the pole placement method, the poles of the closed-loop plant can be appropriately placed to ensure stability, sufficient damping, and lower bandwidth compared to the d-axis current controller. The complete controller is shown in Fig. 7,

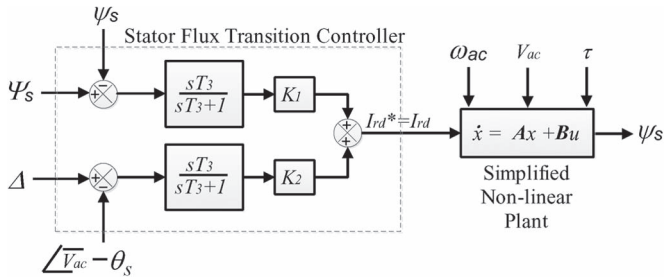

Fig. 7. Nonlinear simplified plant model valid during transition from dc to ac mode as described by (28) with the stator flux transition controller.

where gains K_1 and K_2 correspond to the gains of the stator flux transition controller. High-pass filters are used with time period T_3, equal to the stator time constant, such that the controller is effective only during the mode transition and does not affect the steady-state rotor d-axis current command. This eliminates the effects of inaccuracy in estimation of the ac mode steady-state operating points Ψ_s and Δ. With the designed full state feedback controller, the transition from B to A is without any oscillation as can be seen in Fig. 6. As the input matrix in (29) has a single nonzero element, the control vectors are effective only along the stator flux magnitude axis in the state plane, as shown by arrows in Fig. 6. The rotor d-axis current limiter has a large impact on the allowable damping and, therefore, on the state trajectory. The outputs of the reactive power controller and the stator flux transition controller are summed together to command the rotor d-axis current controller in ac mode.

H. Synchronizer

The appropriate choice of transition instant, commanded by Sw, is the remaining degree of freedom for minimizing the stator flux perturbation during mode transition. The switching instant of the sources in the stator directly affects the initial condition of δ in (28). The starting point on Fig. 6 for δ is set on an *ad hoc* basis to illustrate the effect of the stator flux transition controller on the state trajectory during dc to ac mode transition. This section will discuss on the choice of appropriate instant of transition command Sw to minimize the perturbation in the stator flux and hence in the shaft torque and speed. Two methods are used to illustrate and corroborate the correct transition instance. First, a space vector method will be used to analyze the correct instant of transition. This will be validated using the state plane analysis introduced in the previous section.

1) DC to AC Transition: Assuming that the DFM is operating steadily in dc mode, V_{sd} and V_{sq} are the d-axis and q-axis components of the dc source voltage in the stator flux reference frame, as shown in Fig. 8(a). These components along with the stator flux are stationary in space. The ac voltage vector $V_{\rm ac}$ represents the to-be-connected ac supply. Assuming that the direction of the shaft rotation is counterclockwise, the vector $V_{\rm ac}$ rotates counterclockwise at the ac supply frequency relative to the $d-q$ reference frame.

Assuming that the stator flux magnitude before and after the mode transition is identical, for minimal perturbation of the stator flux magnitude, (3) must be equated to zero during mode transition. This implies that the d-axis component of

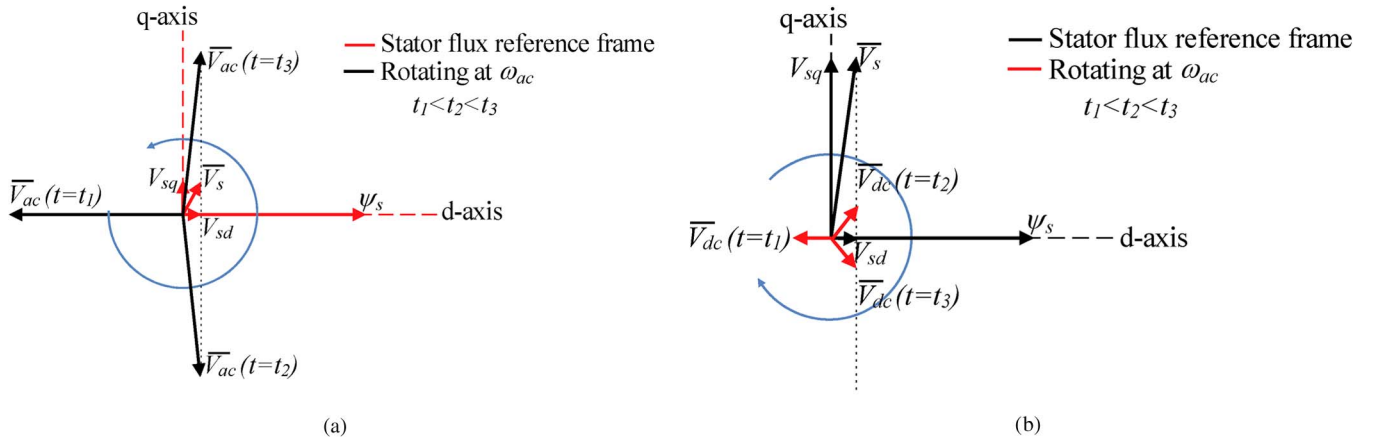

Fig. 8. Determination of the correct instant of transition based on the existing stator voltage, stator flux space vector, and incoming source voltage vector. (a) DC to ac mode transition. (b) AC to dc mode transition.

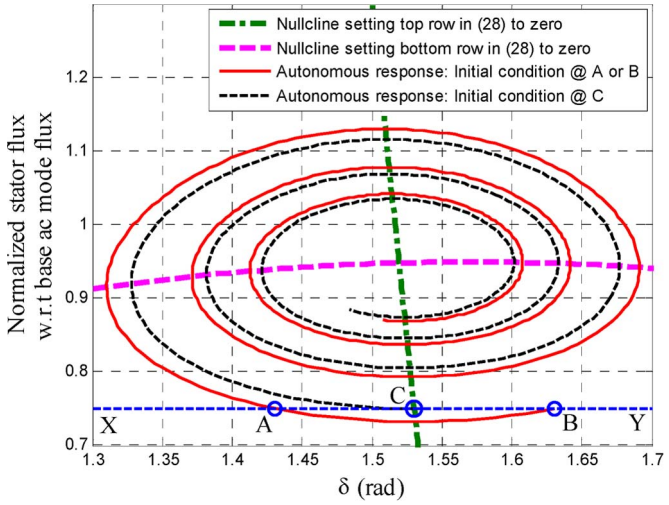

Fig. 9. State plane analysis for finding optimum switching instant during dc to ac mode: the stator flux magnitude swing is minimum when the initial condition in (28) is at C as compared to A or B. The stator flux transition controller is disabled in this analysis. XY: dc mode stator flux magnitude level.

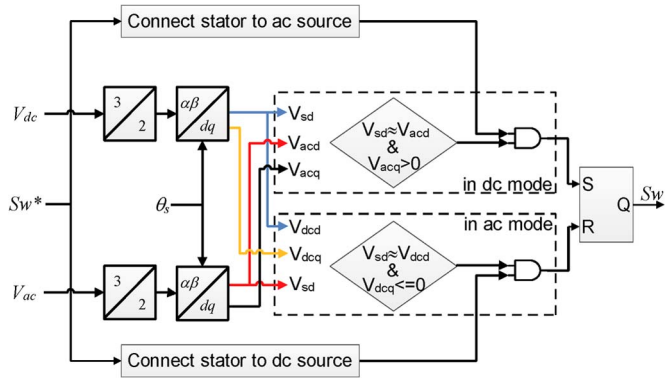

Fig. 10. Flowchart of synchronizer: the shaft speed is compared to the designed transition speed using a hysteresis comparator to compute Sw^*. The correct transition instant command Sw is used to change the stator connection to the source.

the incoming ac voltage must be equal to the existing d-axis voltage, ignoring the effect of the stator resistance. The two instances where the d-axis voltage matches are at t_2 and t_3 in Fig. 8(a). Additionally, the stator flux frequency must transition from zero to the ac supply frequency, which is governed by (6). A positive q-axis component of ac voltage drives the stator flux frequency toward the ac supply frequency. Thus, switching at t_3 ensures that the mode transition is accomplished with minimal disturbance to the stator flux.

A generalized approach based on the state plane analysis can be used to determine the correct transition instant in cases where the stator flux magnitudes in the two modes are unequal. For example, assuming the dc mode stator flux to be 0.75 p.u. as compared to the ac mode stator flux, the switching instant can place the initial condition for the state trajectory anywhere in the line XY in Fig. 9. Without the stator flux transition controller, if the transition instant is set at A or B, the state trajectory makes a larger magnitude swing of the stator flux when compared to the transition instant C. Essentially, C is the intersection of the first null-cline with the dc mode stator flux level. This is the identical condition of equating (3) to zero, as formulated using the space vector method. The second condition of positive q-axis voltage is satisfied by the choice of positive δ.

2) AC to DC Transition: During the ac to dc transition, V_{sd} and V_{sq} are initially the d-axis and q-axis components of the ac voltage in the stator flux reference frame as shown in Fig. 8(b). However, in this case, the incoming dc source voltage vector rotates clockwise at the ac supply frequency relative to the $d-q$ reference frame. Using the same argument as in the dc to ac transition, matching the d-axis component of the incoming dc voltage with V_{sd} and ensuring that the q-axis component of the dc voltage is negative or zero make t_3 the optimal switching instant from ac to dc. The stator flux controller in this case actively controls the stator flux after the transition by rotor d-axis current command and ensures a smooth transition. A similar state plane analysis can be used for determining correct transition instant for drive designs with unequal dc and ac mode stator flux levels.

A flowchart of the synchronizer scheme is shown in Fig. 10, which pulls these two observations about the correct transition instance. Based on the Sw^* command and the correct instant of transition, the binary signal Sw is generated. When the drive is operating in dc mode, a command to connect the stator to the

TABLE I
DFM PARAMETERS

Stator resistance	3.575 Ω
Rotor resistance	4.229 Ω
Stator leakage inductance	9.6 mH
Rotor leakage inductance	9.6 mH
Mutual inductance	165 mH
Moment of inertia	0.01 kgm^2
Frictional coefficient	0.0025 Nm-s/rad

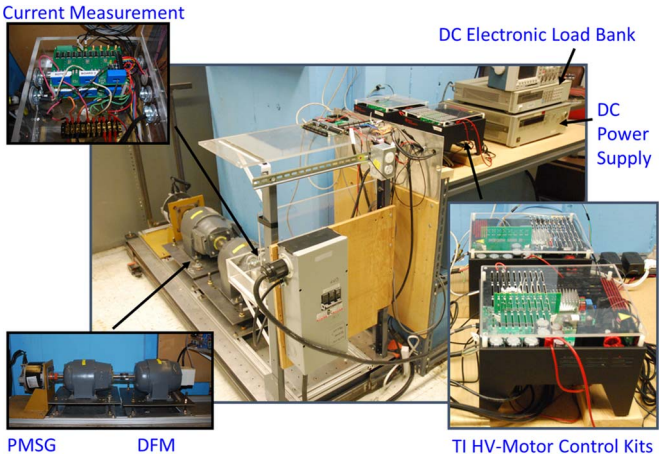

Fig. 11. Experimental setup: Two TI HV Motor Control Kits are used to evaluate the proposed control architecture.

ac source will set the Q bit of the RS-latch. In ac mode, a command to connect the stator to the dc source will reset the bit.

IV. EXPERIMENTAL RESULTS

A 1-hp 220-V/150-V 60-Hz four-pole 1800-r/min DFM has been used to illustrate the control architecture experimentally. The DFM parameters are given in Table I. Two Texas Instruments High Voltage Motor Control & PFC Developer's Kits, named Kit-I and Kit-II, are used for this purpose as shown in Fig. 11. These kits have Intelligent Power module PS-21765 as the power stage with a built-in gate driver [29]. The kits also have programmable Piccolo microcontroller TMS320F28035 with a 32-bit CPU and a 60-MHz clock. The kits are modified to enable reading of relevant measurements like voltages and currents through the built-in 12-bit ADCs. Kit-I is programmed to emulate either an ac source of 134 V, 40 Hz, or a dc source of 20 V through open-loop duty ratio command. The choice of the ac source voltage ensures that the off-the-shelf DFM remains within the rated operating speed. The rotor is connected to Kit-II. The complete control architecture is programmed in the TMS320F28035 microcontroller placed in Kit-II. The mode switching command Sw from Kit-II switches the excitation of Kit-I. Although this would not be the case in an actual implementation where a transfer switch will connect the stator between the dc and ac sources, this setup is chosen for demonstration of the control architecture to ensure a "bumpless" transition. For realistic high-power applications, the inverter topology and modulation technique may be suitably selected based on the availability of the device ratings, allowable harmonic content in the generated waveforms, and allowable converter losses. The DFM is also mechanically coupled to a permanent magnet synchronous generator (PMSG) which is connected to an electronic programmable load bank that can operate in controlled current mode.

A. Experimental Evaluation of the Dynamic Performance of the Overall Controller

For the experimental setup, a speed comparator with hysteresis is used to generate the mode transition command Sw^* to prevent chattering between the two modes, i.e., a dc to ac mode transition is commanded when the rotor speed is above 720 r/min. However, an ac to dc mode transition is commanded when the rotor speed is below 648 r/min. The transition speed selection for the experimental setup takes into account the nonidealities of the prototype DFM like resistances and leakages [30]. The ac supply synchronous speed is 1200 r/min.

1) Performance of the Controller During Acceleration: To evaluate the performance of the complete controller, a step command in speed of 1800 r/min is given at $t = 0$. The measured speed is shown in Fig. 12(a), which undergoes a mode transition at $t = 0.94$ s. As the dc mode torque limit is set to 75% of the ac mode torque, the slope of the speed curve is steeper in ac mode as compared to that in dc mode. Fig. 12(b) illustrates the transition of the estimated stator flux frequency from 0 to 251 rad/s. The transient in the estimated stator flux frequency is critical for providing the feedforward terms of the current controller to ensure proper reference tracking of the individual axis currents. This is shown in Fig. 12(c), where the q-axis reference current is tracked properly by the q-axis feedback current even during mode transition. Perturbations in the stator flux magnitude result in perturbation of the q-axis current reference for a commanded torque. The frequency of these perturbations is on the order of the ac source frequency. Fig. 12(d) shows the A-phase stator and rotor current during acceleration. The stator current is initially dc, which changes to 40 Hz at the transition instant. The rotor current is accordingly controlled from the rotor inverter. The rotor current frequency gradually increases as the rotor speed increases in the dc mode. After the transition to ac mode, the rotor current frequency decreases until the rotor speed reaches ac synchronous speed. This is subsynchronous operation. Beyond this speed, the rotor current frequency increases in the supersynchronous operation again as expected.

The electromagnetic torque during the acceleration is shown in Fig. 13. The torque limit is changed at the DFM stator time constant, ensuring a smooth transfer from the dc to ac mode. Additionally, the acceleration test is repeated with identical dc mode and ac mode torque limits as shown again in Fig. 13. In both cases, the electromagnetic torque undergoes a near "bumpless" transition as the mode changes from the dc to ac mode. The performance of the stator flux transition controller is evaluated during the acceleration test. The estimated stator flux during the dc to ac mode transition is shown in Fig. 14. The top figure shows the comparison of the simplified nonlinear model with that of the experimentally observed without any stator flux transition controller. As expected, the stator flux magnitude oscillates before settling down to the ac mode level

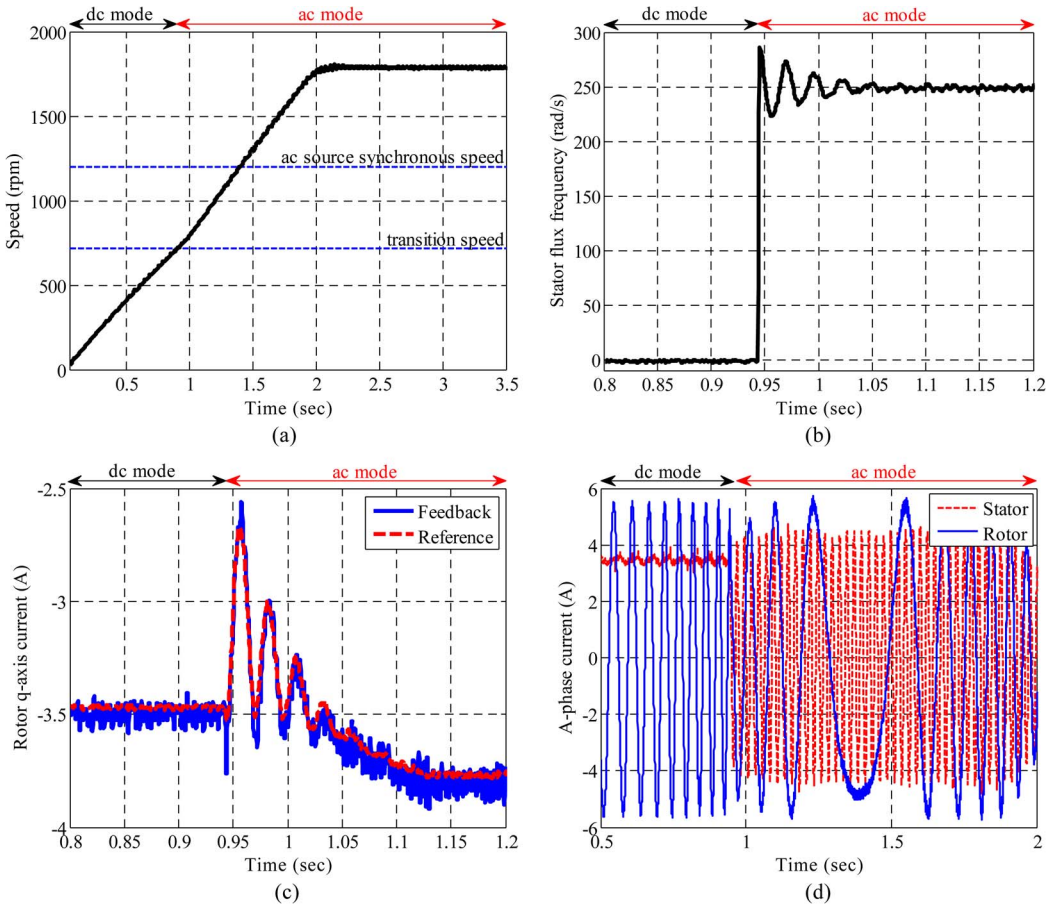

Fig. 12. Experimental results with a step command of 1800 r/min in reference speed with the DFM initially in standstill condition. A dc to ac mode transition occurs at $t = 0.94$ s when the shaft speed crosses the transition speed of 720 r/min. (a) Measured shaft speed. (b) Estimated stator flux frequency at the instant of transition. (c) Tracking of the q-axis current at the transition instant; the reference is set by the speed controller. (d) Measured stator and rotor A-phase currents; while the stator current changes from dc to a 40 Hz ac at transition, rotor current is precisely controlled to ensure a bumpless transition.

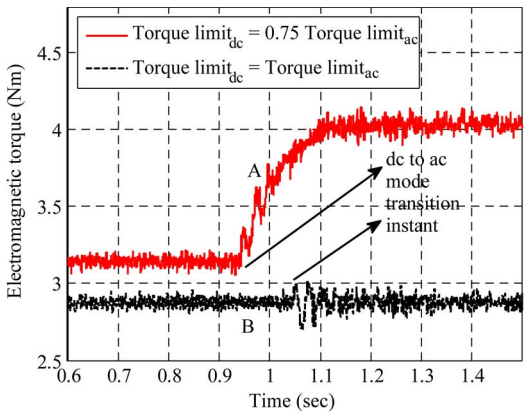

Fig. 13. Experimental results: the electromagnetic torque for the DFM during dc to ac transition instant. (A) With different torque capabilities of the DFM in the dc and ac mode. (B) With identical torque capability of the DFM drive in the dc and ac mode.

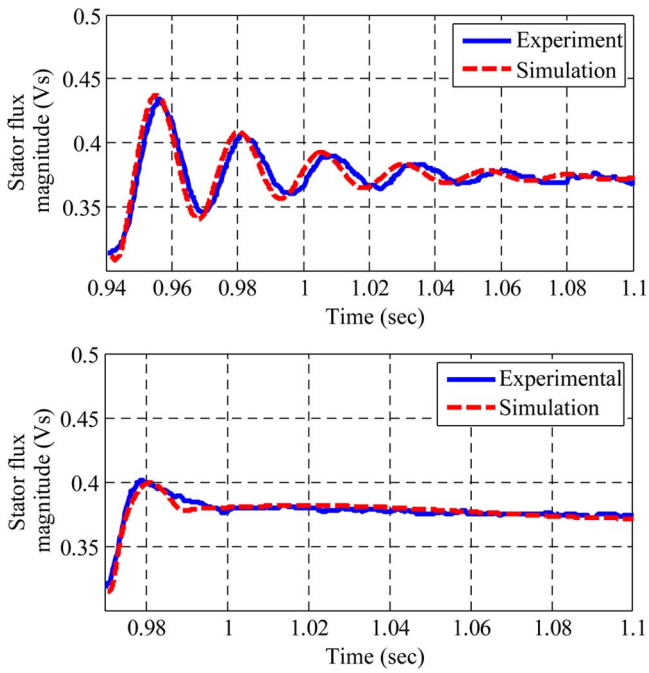

Fig. 14. Experimental results: comparison of stator flux transition with simulation using the nonlinear simplified model of the plant during dc to ac mode transition. (Top) Without stator flux transition controller. (Bottom) With stator flux transition controller.

as determined by the ac source, equivalent to the spiral in Fig. 6. With an effective stator flux transition controller, the stator flux settles to the ac mode level faster and without oscillation.

2) Performance of the Controller During Deceleration and Reactive Power Control: The speed response of the DFM drive when a step command of 0 r/min is set as reference while the DFM is initially operating at 1800 r/min is shown in Fig. 15(a).

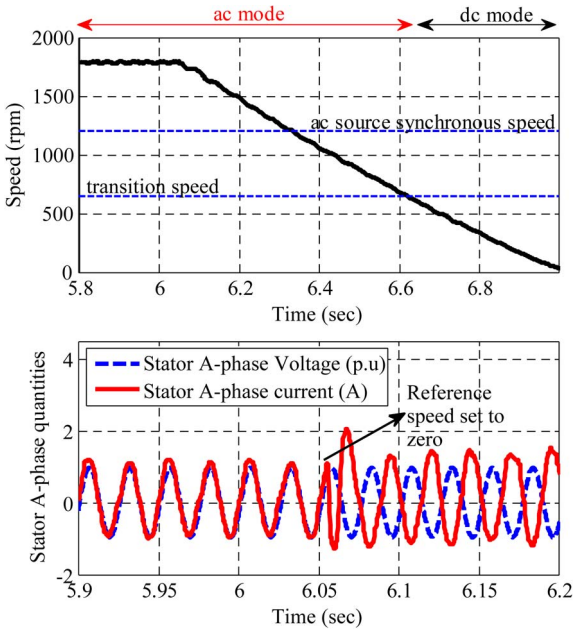

Fig. 15. Experimental results: the reference speed is set to zero at $t = 6.06$ s with initially the DFM running at 1800 r/min. The transition speed is set as 648 r/min, below which dc mode is engaged. (Top) Measured shaft speed. (Bottom) Evaluation of the stator reactive power controller before and after the step change in reference speed.

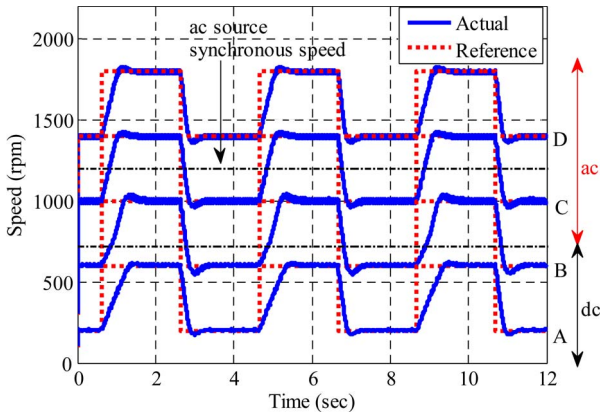

Fig. 16. Experimental results: reference tracking of speed controller in three speed ranges. (A) DC mode only. (B) DC and ac modes. (C) AC mode only (sub- and supersynchronous). (D) AC mode only (supersynchronous).

In this case, the ac to dc mode transition speed is effective at 648 r/min. The reactive power controller in ac mode ensures that the stator voltage and current are in phase, as seen in the A-phase waveforms in Fig. 15(b). With sudden braking as commanded by setting the reference speed to zero, the active power to the stator reverses. The reactive power controller ensures a 180° phase between the stator A-phase voltage and current.

B. Dynamic Performance of the Controller for Reference Speed Tracking

To verify the dynamic performance of the proposed drive, four sets of alternating reference speed commands are given as inputs to the controller as shown in Fig. 16. First, the reference speed alternates between 200 and 600 r/min (corresponding to waveform A). This regime is entirely in dc mode. In the second set, the reference speed alternates between 600 and 1000 r/min (corresponding to waveform B). In this case, the controller switches between ac and dc modes based on the actual speed. In the third set, the reference speed alternates between 1000 and 1400 r/min (corresponding to waveform C). This regime is entirely in ac mode. As the ac synchronous speed is 1200 r/min, in this case, the rotor operates in between subsynchronous and supersynchronous regions. Finally, the reference speed alternates between 1400 and 1800 r/min (corresponding to waveform D). As the dc mode torque limit is set to a lower value compared to that of the ac mode, the slope of the speed response in A is lower compared to that in C and D, as shown in Fig. 16. For B, the slope of the speed response changes similar to that as observed in Fig. 12(a).

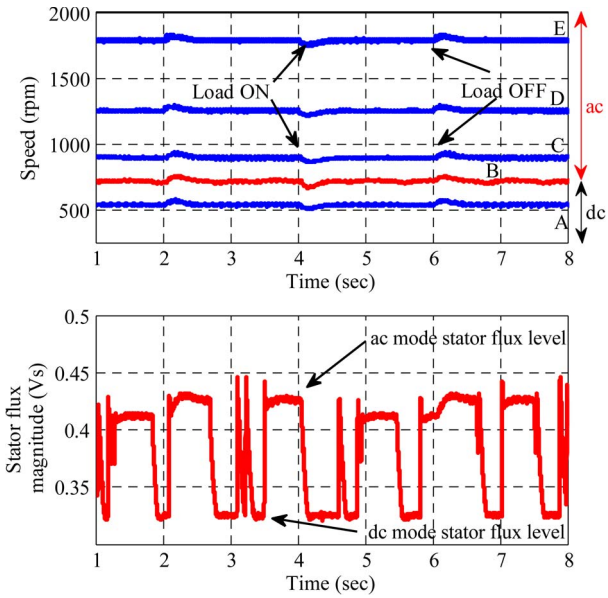

Fig. 17. Experimental results: load torque disturbance rejection at constant commanded speed under different operating modes. (Top) Rotor speed—(A) Commanded speed 540 r/min (dc mode only). (B) Commanded speed 720 r/min (dc and ac modes). (C) Commanded speed: 900 r/min (ac mode only, subsynchronous). (D) Commanded speed: 1250 r/min (ac mode only, near synchronous). (E) Commanded speed: 1800 r/min (ac mode only, supersynchronous). (Bottom) Perturbation in stator flux magnitude between dc and ac mode levels as the drive operates at the transition speed. The hysteresis comparator that generates Sw^* is replaced with a single mode transition speed of 720 r/min [corresponding to rotor speed profile (B) in (a)].

C. Performance of the Controller Under Load Disturbance

In order to verify the disturbance rejection of the proposed drive under sudden load torque variations, the programmable load bank connected to the DFM-driven PMSG is used. The reference speed is set to (A) 540, (B) 720, (C) 900, (D) 1260, and (E) 1800 r/min, as shown in Fig. 17(a). The electronic load bank is programmed to turn on and off at a frequency of 0.5 Hz in constant current mode. Sudden change in the electrical load of the PMSG changes the load torque at the DFM shaft. The speed response of the DFM drive is tightly controlled near the reference speed. The PMSG offers more shaft torque loading at a higher speed since the terminal voltage of the PMSG is proportional to the shaft speed. In this experiment, power drawn by the electronic load bank under different operating

speeds are (A) 60, (B) 80, (C) 100, (D) 140, and (E) 200 W. For case (B), the hysteresis comparator of the speed for mode transition is deliberately replaced with a single transition speed of 720 r/min. This compels the drive to operate in the dc and ac mode erratically as can be seen by the stator flux magnitude oscillating between the dc mode level and the ac mode level in Fig. 17(b). Even operating right at the transition speed, the rotor speed is controlled tightly at the desired speed irrespective of the operating mode and load variations.

V. Conclusion

This paper has discussed and demonstrated the control architecture for a switched DFM suitable for a propulsion application where both ac and dc power are available. With a proper choice of transition speed, the proposed configuration can enable full speed range for the drive with minimal power electronics. The results show that the proposed controller works equivalently under the tested operating conditions (dc mode, ac mode, and during transitions between ac and dc modes). The results also validate the operation of the stator flux estimator, synchronizer, reactive power controller, and stator flux transition controller. A more robust controller may include an online parameter estimation scheme not only to update the DFM parameters but also to tune the controller for variable load friction and inertia. Finally, proper switching between dc and ac modes and a controlled flux transition with reactive power control (in ac mode) open up opportunities for system level design choices to be made that can minimize weight and cost of the propulsion drive.

References

[1] J. S. Chalfant, C. Chryssostomidis, and M. G. Angle, "Study of parallel ac and dc electrical distribution in the all-electric ship," in *Proc. Conf. Grand Challenges Model. Simul.*, 2010, pp. 319–326.

[2] R. Pena, J. C. Clare, and G. M. Asher, "Doubly-fed induction generator using back-to-back PWM converters and its application to variable-speed wind-energy generation," *Proc. Inst. Elect. Eng.—Elect. Power. Appl.*, vol. 143, no. 3, pp. 231–241, May 1996.

[3] F. Blaabjerg, M. Liserre, and K. Ma, "Power electronics converters for wind turbine systems," *IEEE Trans. Ind. Appl.*, vol. 48, no. 2, pp. 708–719, Mar./Apr. 2012.

[4] H. Akagi and H. Sato, "Control and performance of a doubly-fed induction machine intended for a flywheel energy storage system," *IEEE Trans. Power Electron.*, vol. 17, no. 1, pp. 109–116, Jan. 2002.

[5] L. Ran, D. Xiang, and J. L. Kirtley, Jr., "Analysis of electromechanical interactions in a flywheel system with a doubly fed induction machine," *IEEE Trans. Ind. Appl.*, vol. 47, no. 3, pp. 1498–1506, May/Jun. 2011.

[6] Y. Kawabata, E. Ejiogu, and T. Kawabata, "Vector-controlled double inverter-fed wound-rotor induction motor suitable for high-power drives," *IEEE Trans. Ind Appl.*, vol. 35, no. 5, pp. 1058–1066, Sep./Oct. 1999.

[7] G. Poddar and V. T. Ranganathan, "Sensorless field-oriented control for double-inverter-fed wound-rotor induction motor drive," *IEEE Trans. Ind. Electron.*, vol. 53, no. 1, pp. 1089–1096, Feb. 2006.

[8] M. Abdellatif, M. Debbou, I. Slama-Belkhodja, and M. Pietrzak-David, "Simple low-speed sensorless dual DTC for double fed induction machine drive," *IEEE Trans. Ind. Electron.*, vol. 61, no. 8, pp. 3915–3922, Aug. 2014.

[9] F. Bonnet, P.-E. Vidal, and M. Pietrzak-David, "Dual direct torque control of doubly fed induction machine," *IEEE Trans. Ind. Electron.*, vol. 54, no. 5, pp. 2482–2490, Oct. 2007.

[10] Y. Liu and L. Xu, "The dual-current-loop controlled doubly fed induction motor for EV/HEV applications," *IEEE Trans. Energy Convers.*, vol. 28, no. 4, pp. 1045–1052, Dec. 2013.

[11] M. S. Vicatos and J. A. Tegopoulos, "A doubly-fed induction machine differential drive model for automobiles," *IEEE Trans. Energy Conver.*, vol. 18, no. 2, pp. 225–230, Jun. 2003.

[12] L. Morel, H. Godfroid, A. Mirzaian, and J.-M. Kauffmann, "Double-fed induction machine: Converter optimisation and field oriented control without position sensor," *Proc. Inst. Elect. Eng.—Elect. Power Appl.*, vol. 145, no. 4, pp. 360–368, Jul. 1998.

[13] J.-K. Lung, Y. Lu, W.-L. Hung, and W.-S. Kao, "Modeling and dynamic simulations of doubly fed adjustable-speed pumped storage units," *IEEE Trans. Energy Convers.*, vol. 22, no. 2, pp. 250–258, Jun. 2007.

[14] S. B. Leeb *et al.*, "How much dc power is necessary?" *Nav. Eng. J.*, vol. 122, no. 2, pp. 79–92, Jun. 2010.

[15] R Fischer and K. Yankaskas, "Noise control on ships-enabling technologies," Office Naval Res., Arlington, VA, USA, 2011.

[16] A. Tapia, G. Tapia, J. Ostolaza, and J. Saenz, "Modeling and control of a wind turbine driven doubly fed induction generator," *IEEE Trans. Energy Convers.*, vol. 18, no. 2, pp. 194–204, Jun. 2003.

[17] B. Hopfensperger, D. J. Atkinson, and R. A. Lakin, "Stator-flux-oriented control of a doubly-fed induction machine with and without position encoder," *Proc. Inst. Elect. Eng.—Elect. Power Appl.*, vol. 147, no. 4, pp. 241–250, Jul. 2000.

[18] A. Petersson, L. Harnefors, and T. Thiringer, "Comparison between stator-flux and grid-flux-oriented rotor current control of doubly-fed induction generators," in *Proc. 35th IEEE PESC*, Aachen, Germany, 2004, vol. 1, pp. 482–486.

[19] L. Xu and W. Cheng, "Torque and reactive power control of a doubly fed induction machine by position sensorless scheme," *IEEE Trans. Ind. Appl.*, vol. 31, no. 3, pp. 636–642, May/Jun. 1995.

[20] R. Cardenas, R. Pena, S. Alepuz, and G. Asher, "Overview of control systems for the operation of DFIGs in wind energy applications," *IEEE Trans. Ind. Electron.*, vol. 60, no. 7, pp. 2776–2798, Jul. 2013.

[21] A. Boglietti, A. Cavagnino, M. Popescu, and D. Staton, "Thermal model and analysis of wound-rotor induction machine," *IEEE Trans. Ind. Appl.*, vol. 49, no. 5, pp. 2078–2085, Sep./Oct. 2013.

[22] A. K. Jain and V. T. Ranganathan, "Modeling and field oriented control of salient pole wound field synchronous machine in stator flux coordinates," *IEEE Trans. Ind. Electron.*, vol. 58, no. 3, pp. 960–970, Mar. 2011.

[23] S. Muller, M. Deicke, and R. W. De Doncker, "Doubly fed induction generator systems for wind turbines," *IEEE Ind. Appl. Mag.*, vol. 8, no. 3, pp. 26–33, May/Jun. 2002.

[24] J. A. Sayago, T. Bruckner, and S. Bernet, "How to select the system voltage of MV drives—A comparison of semiconductor expenses," *IEEE Trans. Ind. Electron.*, vol. 55, no. 9, pp. 3381–3390, Sep. 2008.

[25] W. Leonhard, *Control of Electrical Drives*. Berlin, Germany: Springer-Verlag, 1985.

[26] N. R. N. Idris and A. H. M. Yatim, "An improved stator flux estimation in steady-state operation for direct torque control of induction machines," *IEEE Trans. Ind. Appl.*, vol. 38, no. 1, pp. 110–116, Jan./Feb. 2002.

[27] G. D. Marques and D. M. Sousa, "Stator flux active damping methods for field-oriented doubly fed induction generator," *IEEE Trans. Energy Convers.*, vol. 27, no. 3, pp. 799–806, Sep. 2012.

[28] S. H. Strogatz, *Nonlinear Dynamics and Chaos*. Reading, MA, USA: Addison-Wesley, 1994.

[29] High Voltage Motor Control and PFC Developer's Kit. [Online]. Available: http://www.ti.com/tool/TMDSHVMTRPFCKIT

[30] A. Banerjee, M. S. Tomovich, S. B. Leeb, and J. L. Kirtley, Jr., "Power converter sizing for a switched doubly fed machine propulsion drive," *IEEE Trans. Ind. Appl.*, vol. 51, no. 1, pp. 248–258, Jan./Feb. 2015.

Arijit Banerjee (S'12) received the B.E. degree in electrical engineering from Bengal Engineering and Science University, Howrah, India, in 2005 and the M.Tech. degree in electrical engineering from the Indian Institute of Technology, Kharagpur, India, in 2007. He is currently working towards the Ph.D. degree at the Massachusetts Institute of Technology, Cambridge, MA, USA.

In 2006–2007, he was a visiting student at the Institute for Power Electronics and Control of Drives, Technische Universität Darmstadt, Darmstadt, Germany, under the DAAD Fellowship. From 2007 to 2011, he was with the Power Conversion Systems Group, General Electric Global Research Centre, Bangalore, India, where he was working on monitoring and diagnostics of electromechanical systems using electrical signatures. In 2011, he joined the Laboratory for Electromagnetic and Electronic Systems, Massachusetts Institute of Technology. He is the holder of ten issued patents and several patent applications. His research interests include the analysis, design, control, and diagnostics of electromechanical systems.

Michael S. Tomovich (S'12) received the B.S. degree in electrical and computer engineering from Carnegie Mellon University, Pittsburgh, PA, USA, in 2011 and the S.M. degree in electrical engineering and computer science from Massachusetts Institute of Technology, Cambridge, MA, USA, in 2014, where his research was in power electronics and motor control.

He worked with Team Astrobotic in pursuit of the Google Lunar X Prize. He was also a member of the MIT Global Founders Skills Accelerator in the summer of 2013. His interests include embedded systems, power electronics, and entrepreneurship.

Steven B. Leeb (F'07) received the Ph.D. degree from Massachusetts Institute of Technology (MIT), Cambridge, MA, USA, in 1993.

He has served as a commissioned officer in the USAF reserves, and he has been a member of the faculty of the Department of Electrical Engineering and Computer Science, MIT, since 1993. He also holds a joint appointment with the Department of Mechanical Engineering, MIT. He is currently a MacVicar Fellow and a Professor of electrical engineering and computer science with the Laboratory for Electromagnetic and Electronic Systems. In his capacity as a Professor at MIT, he is concerned with the design, development, and maintenance processes for all kinds of machinery with electrical actuators, sensors, or power electronic drives. He is the author or coauthor of over 80 publications and 13 U.S. patents in the fields of electromechanics and power electronics.

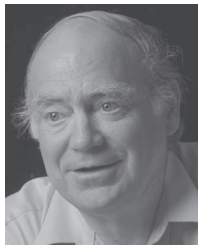

James L. Kirtley, Jr. (S'69–M'71–SM'80–F'91–LF'11) received the Ph.D. degree from Massachusetts Institute of Technology (MIT), Cambridge, MA, USA, in 1971.

He is a Professor of electrical engineering with MIT. He served as an Electrical Engineer with the Large Steam Turbine Generator Department, General Electric, and as Vice President and General Manager of the Tech Center and as Chief Scientist and as Director with Satcon Technology Corporation. He was a Gastdozent with the Swiss Federal Institute of Technology, Zürich, Switzerland. He is a member of the Editorial Board of *Electric Power Components and Systems*. He is a specialist in electric machinery and electric power systems.

Dr. Kirtley is a Registered Professional Engineer in the State of Massachusetts. He was the Editor-in-Chief of the IEEE TRANSACTIONS ON ENERGY CONVERSION from 1998 to 2006, which he continues to serve as an Editor. He was awarded the IEEE Third Millennium Medal in 2000 and the Nikola Tesla Prize in 2002. He was elected to the United States National Academy of Engineering in 2007.